Three-Dimensional Self-Assembling of Gold Nanorods with Controlled Macroscopic Shape and Local Smectic B Order

Cyrille Hamon,[†] Marie Postic,[‡] Elsa Mazari,[§] Thomas Bizien,[†,‡] Christophe Dupuis,[§] Pascale Even-Hernandez,[†] Angela Jimenez,[‡] Laurent Courbin,[‡] Charlie Gosse,[§] Franck Artzner,[‡] and Valérie Marchi-Artzner[†,*]

[†]Institut des Sciences Chimiques de Rennes, UMR 6226 CNRS, Université Rennes 1, Avenue du Général Leclerc, 35042 Rennes Cedex, France, [‡]Institut de Physique de Rennes, UMR 6251 CNRS, Université Rennes 1, Avenue du Général Leclerc, 35042 Rennes Cedex, France, and [§]Laboratoire de Photonique et de Nanostructures, LPN-CNRS, Route de Nozay, 91460 Marcoussis, France

ABSTRACT

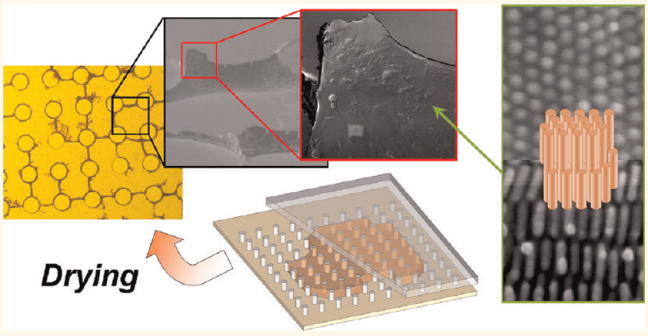

We describe a method of controlled evaporation on a textured substrate for self-assembling and shaping gold-nanorod-based materials. Tridimensional wall features are formed over areas as large as several square millimeters. Furthermore, analyses by small-angle X-ray scattering and scanning electron microscopy techniques demonstrate that colloids are locally ordered as a smectic B phase. Such crystallization is in fact possible because we could finely adjust the nanoparticle charge, knowledge that additionally enables tuning the lattice parameters. In the future, the type of ordered self-assemblies of gold nanorods we have prepared could be used for amplifying optical signals.

KEYWORDS: gold nanorods · self-assembly · 3D crystal · shaping · PEGylated alkanethiolate · superstructure · controlled drying · PDMS stamp · SAXS · SEM

Gold nanorods (GNRs) are promising components for nanosystems dedicated to applications in fields such as sensing, imaging, and diagnostics.[1−5] Indeed, they are particularly attractive because of their unique optical properties and their ability to self-organize, both features originating from their shape anisotropy.[6−12] Ordered assemblies of such metal nanoparticles are for instance used for amplification of optical signals in fluorescence,[13] Raman,[14−16] and absorption spectroscopies.[17,18] Plasmon coupling leads to collective surface plasmon resonances that can be adjusted over a wide spectral domain by tuning the objects' shape and size as well as their interdistance.[19,20] Different methods have been exploited to prepare three-dimensional (3D) structures made of GNRs,[21] by either association in solution,[9,22,23] drying at an interface,[12,24,25] or templating.[2,26] Nevertheless, most of these processes yield colloidal crystals having a size limited to a few micrometers, a poorly defined shape, and an inhomogeneous thickness. Furthermore, methods relying on drying generally lack control with respect to spacing between the deposited particles.

The present paper describes a novel drying method where GNR crystallization is managed in order to obtain a macroscopic material having both a predetermined crystalline structure and a predetermined shape. As self-assembling is governed by the balance between van der Waals,[27] depletion,[17,28,29] and electrostatic interactions,[30] finely tuning the particle chemical coating is of foremost importance to find a compromise between attractive and repulsive forces. To that effect, we here exchange the detergent present at the gold surface after synthesis for a combination of neutral and negative alkanethiolates. Using such a mixture should allow us to adjust the colloid interdistance in the final material. In parallel, we develop a technique to guide the drying of the GNR suspension over areas as large as several square millimeters. A topographically patterned polydimethylsiloxane

* Address correspondence to valerie.marchi-artzner@univ-rennes1.fr.

Received for review February 9, 2012 and accepted April 12, 2012.

Published online April 12, 2012
10.1021/nn3006027

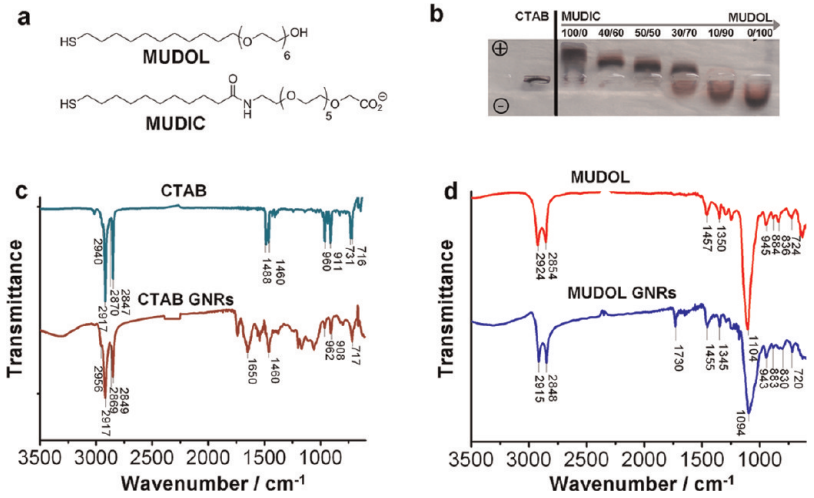

Figure 1. (a) Chemical structures of the MUDOL and MUDIC ligands. (b) Gel electrophoresis of GNRs grafted with different MUDIC/MUDOL mixtures. CTAB denotes the "as-synthetized" sample, *i.e.*, before any ligand exchange. (c, d) FTIR spectra of lyophilized GNRs grafted with either CTAB or MUDOL. Before analysis, the ligand excess was removed by dialysis. Spectra of the pure capping agents are displayed as references, the curves being shifted for the sake of clarity.

(PDMS) mold sealed on a smooth substrate is used both to regulate water evaporation and to control the deposition of the GNRs in given locations thanks to contact line pinning. Our results demonstrate possibilities for engineering 3D walls made of nanometer rodlike particles arranged on 3D arrays. The fabricated self-assembled superstructures are imaged using scanning electron microscopy (SEM), which reveals the presence of crystallized domains obeying a smectic B order. Besides, complementary experiments that include bulk drying in capillary tubes and small-angle X-ray scattering (SAXS) analysis permit us to supplement the previously acquired structural data. In addition, we succeed in varying the lattice parameter of the colloidal crystal by changing the amount of negatively charged alkanethiolates contained in the nanoparticle capping layer.

RESULTS AND DISCUSSION

GNRs are synthesized and subsequently chemically functionalized in order to modulate their interaction potential and therefore to facilitate their self-organization into a structured material. More precisely, colloids are first prepared according to an already published seedless method.[31−33] Their length and diameter are estimated to be respectively 22.0 ± 5.1 and 7.0 ± 2.5 nm, as determined by transmission electron microscopy (TEM; see Figures S1 and S4a) and further confirmed by measurements using wide-angle X-ray scattering (WAXS; see Figure S2). When produced following the above classical synthesis protocol, particles become stabilized against aggregation because cetyl trimethyl ammonium bromide (CTAB) is present in solution. Indeed, this detergent has been dissolved at 0.2 M in the reactive mixture to generate the anisotropic growth of the gold crystals.[31,34] The nanorod surface is in fact coated by a bilayer of interdigitated CTAB molecules, which results in a strong positive charge. Hence, one further needs to cancel the associated repulsive force to achieve a close packing of the colloids during drying.[17] In this context, two main strategies have been developed. On one hand, it is possible to lower the electrostatic interaction by adding salts, which helps screening charges;[8,35,36] on the other hand, some attractive potential can be induced thanks to specific[37−40] or nonspecific linkers,[23] the latter ones being either negative or neutral.[7,41,42] It should be noted that ordered structures of CTAB GNRs have also been evidenced by TEM in the absence of any additive. Yet, in this case self-assembling required a detergent concentration around 20 mM, *i.e.*, much higher than the critical micelle concentration (CMC) (1 mM).[43] Consequently, the presence of CTAB is synonymous with restricted modularity and imprecise control over the interactions between nanorods. This molecule also exhibits additional drawbacks, such as tendencies to denaturate sensitive biological products and to electrostatically adsorb on a broad variety of substrates. Accordingly, we have selected PEGylated alkanethiolate ligands to replace CTAB as stabilizing agents attached to the surface of the metal particles.[44] The commercially available (1-mercaptoundec-11-yl)hexa(ethylene glycol), denoted MUDOL,[45] is here used pure or mixed with a (1-mercaptoundec-11-yl)hexa(ethylene glycoyl)carboxylic acid, denoted MUDIC, and synthesized as described in the literature.[46] Whereas the former molecule is neutral, the latter bears a negative charge at pH close to neutrality (see Figure 1a). The MUDOL ligand appeared attractive for GNR self-assembling, as the PEG spacer would introduce enough repulsive steric forces to balance the attractive dipole−dipole ones during crystallization. Eventually, the addition of an increasing ratio of negatively charged MUDIC will permit modulating the

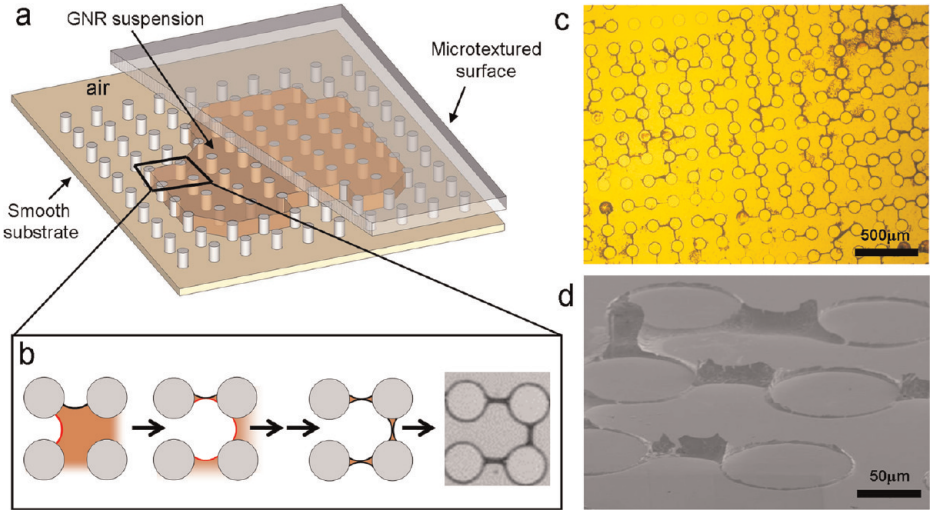

Figure 2. (a) Schematic view of the drying method used to fabricate macroscale GNR self-assemblies. The particle suspension is first confined between a smooth substrate and a PDMS stamp. After water evaporation and removal of the elastomeric mold, an array of solid structures is obtained. (b) Scheme of a typical dewetting process at the scale of four posts; capillary bridges are formed and further dehydrate to yield the colloidal material. (c) Bright field optical micrograph and (d) SEM image of walls made of nanorods.

repulsive interaction in order to adjust the final interparticle spacing.

As already noticed, crude GNRs are obtained as a suspension in 0.2 M CTAB. Hence, the latter concentration has to be reduced before proceeding to any ligand exchange. Purification by several centrifugation/redispersion cycles was undertaken, and the detergent titer was adjusted at ~0.5 mM, *i.e.*, below its CMC value. The substitution of the capping agent could then be achieved and investigated by UV−vis absorbance, IR spectroscopy, electrophoresis, and zetametry. During the exchange of CTAB for MUDOL, the intensity maximum of the longitudinal plasmon band is red-shifted from 763 to 788 nm (see Figure S3), a phenomenon that can be attributed to some modifications in the nanorods' environment. Furthermore, clear alterations are also visible in Fourier transform infrared (FTIR) data (see Figure 1c and d). After substitution, two of the characteristic peaks observed for CTAB GNRs, corresponding to the CH_3 stretching vibrations in the trimethyl ammonium, *antisym* at 2956 cm^{-1} and *sym* at 2869 cm^{-1}, have disappeared. In contrast, the spectrum of the MUDOL particles exhibits bands similar to those of the free MUDOL, particularly in the CH stretching region, between 945 and 720 cm^{-1}, as well as in the $O-CH_2$ stretching region, at 1100 cm^{-1}. Moreover, the positions of the CH_2 stretching bands, *antisym* at 2924 cm^{-1} and *sym* at 2854 cm^{-1}, are shifted to 2915 and 2848 cm^{-1}, respectively. This change is in agreement with the crystallization of the MUDOL alkyl chains around GNRs. Indeed, the energy of the CH_2 stretching transitions has been reported to be a sensitive indicator of the order in alkyl chains since it depends on the incidence of the gauche conformation effects.[47] FTIR data thus suggest that CTAB is exchanged for MUDOL and that the latter molecules are densely packed at the gold surface. Next, to control the electrostatic repulsion between colloids, the positive CTAB was exchanged for various mixtures of neutral MUDOL and negative MUDIC. As a consequence, agarose gel electrophoresis appears to be a pertinent technique to reveal differences in nanorod surface charge (see Figure 1b). When using only MUDOL, particles move toward the negatively charged electrode, which can be attributed to the residual presence of CTAB molecules at the interface. Noticeably, the fact that migration was clearly demonstrated confirms ligand substitution because CTAB GNRs are well-known to aggregate in loading pits due to their low colloidal stability.[36,48] Furthermore, by increasing the ratio of negatively charged MUDIC in the capping layer, we noticed that the particle charge progressively vanished and then reversed. Some of these effects were qualitatively confirmed by measurements of the GNR surface zeta potential, which varies from +55 mV in the case of "as-synthesized" CTAB nanorods to +8 mV for colloids functionalized with pure MUDOL and purified from excess reagent.

In order to incorporate 3D GNR crystals into devices, one first has to self-assemble them on a substrate that enables easy handling and further processing. Additionally, it would also be beneficial to spatially direct material growth in any desired macroscopic shape.[49−51] As a proof of concept, we here rely on microtextured surfaces made of polydimethylsiloxane, similar to the ones that are used to achieve specific hydrodynamic or wetting effects (*e.g.*, the polygonal spreading of a drop).[52] More specifically, cylindrical microposts of height 35 μm and diameter 100 μm were arranged on a square array whose lattice parameter is

175 μm (see Figure 2a). A 1 μL droplet of $\sim 10^{-6}$ M pure MUDOL GNR suspension is confined between a smooth surface (silicon wafer, ITO, or gold-coated glass slide) and the elastomeric stamp before being allowed to dry at room temperature for 10 h (see Figure 2a). In addition to the already present 0.5 mM CTAB, the colloidal solution also contains 0.1 mM Tween 20 so as to improve the degree to which the substrate is wet by the liquid. After complete water evaporation, the PDMS template is removed to yield brown traces over the whole area previously covered by the liquid.

The features present on the sample are characterized at different scales using bright field optical microscopy and SEM. Images show regular patterns, as high as the stamp is deep. They consist of linear walls connected to rings; the former are reminiscent of pinned capillary bridges, while the latter correspond to the column footprints (see Figure 2b–d). When a drop of the same colloidal suspension is dried without confinement, *i.e.*, without applying any PDMS mold, we observe stains made of disordered nanorods, limited in both height and size to a few micrometers and tens of micrometers, respectively (see Figure S5); these results concur with previously published investigations.[45,53] In another complementary experiment, the interdistance between pillars is changed so that the shape of the contact lines and the final morphology of the deposited solid can be altered. Increasing the square lattice parameters from 175 to 350 μm yields tetrapod features in between groups of four adjacent posts instead of simple walls joining two closest neighbors (compare Figure 2c and Figure S13a–c). Patterns are also broader and higher due to the shorter contour length associated with the new geometry. Nevertheless, the nanoscale architecture seems preserved (compare Figure 3a below and Figure S13d). Finally, it is worth noticing that in all cases the presence of Tween 20 is critical to stabilize the liquid bridges between pillars. Indeed in a control experiment where this neutral detergent was omitted, almost no wall was formed (see Figure S6). This research, being mainly dedicated to the control of colloidal assembly through surface charge tuning, the physical mechanisms controlling the drying process, and the subsequent formation of the superstructures, will be published elsewhere.

High-magnification SEM views show that GNRs are densely packed within walls (see Figure 3). Indeed, during the liquid-film thinning colloids are concentrated toward the triple contact line, at the junction between the air, the solution, and the substrate. Seen along their main axis, nanorods appear to follow a hexagonal order, with monodomains larger than 1 μm^2 (see Figure 3a and b). To subsequently investigate the internal structure of the produced solid, we have adopted three different approaches: either defects on the surface were observed (see Figure 3c and d), or the substrate was cleaved perpendicularly to a wall

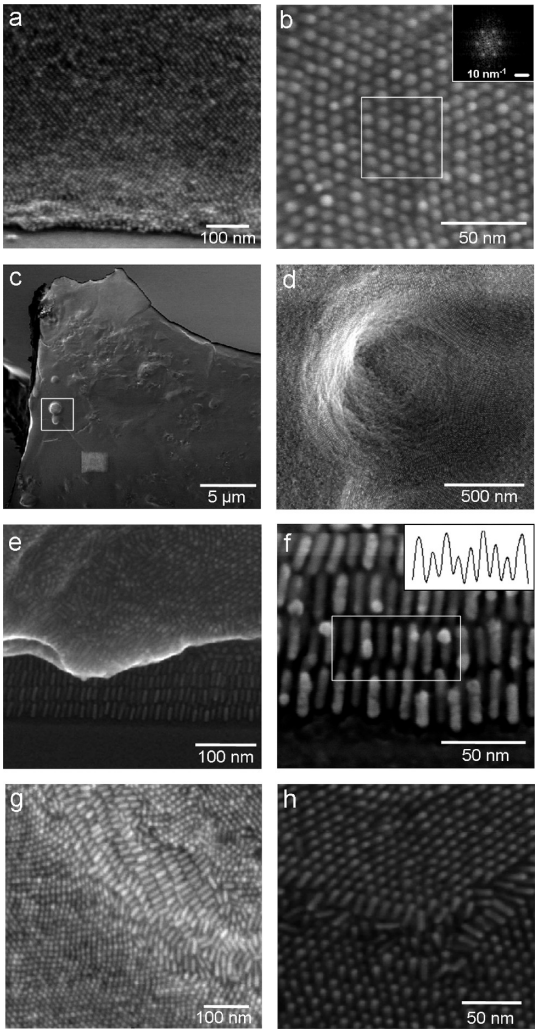

Figure 3. SEM images of the structures obtained from drying between a silicon substrate and a PDMS mold a suspension of pure MUDOL GNRs. (a, b) Hexagonal packing at the wall surface. Fourier analysis was performed on a $\sim 50 \times 50$ nm^2 area. (c, d) Investigation of a concave defect. The cavity displays several micrometer sized smectic B domains. (e, f) Lamellar organization at the substrate vicinity revealed due to substrate cleaving. The intensity profile is plotted along a single nanorod layer. (g, h) Unambiguous smectic B ordering imaged after resection of a part of the solid with micromanipulators.

(see Figure 3e and f), or a part of the latter superstructure was removed with a micrometer-size tool (see Figure 3g and h as well as Figure S7). In all three cases, lamellae made of GNRs arranged side-by-side are evidenced. However, only images of fractures performed with the micromanipulator allow one to obtain both top and side views, which unambiguously reveal the smectic B (SmB) nature of the created colloidal crystal (see Figure 3g and h). Interestingly, in the vicinity of both the substrate and the former air/solution interface, particles are especially well-organized; they all stand perpendicular to the surface (see Figure 3e). A quantitative analysis of these images is next provided. By displaying six peaks perfectly

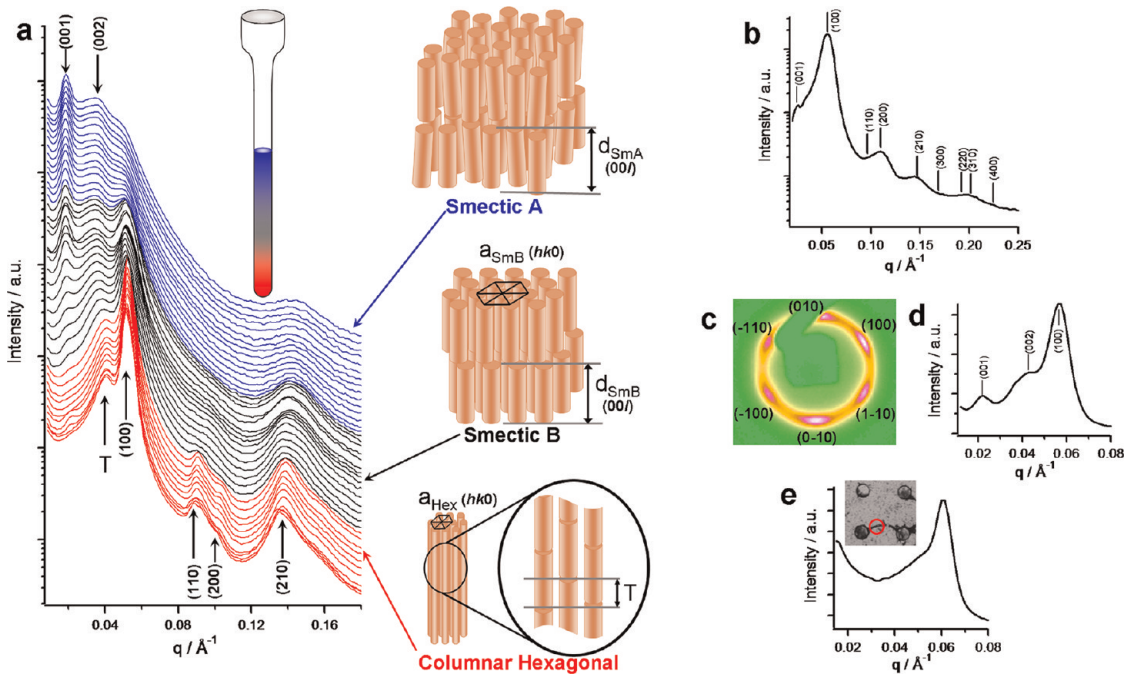

Figure 4. SAXS spectra of a MUDOL GNR suspension dried in a capillary. (a) Data acquired on the SWING beamline at SOLEIL ~12 h after the onset of evaporation. Measurements were performed at different positions along the longitudinal axis of the tube, hence evidencing three different organizations: a columnar hexagonal phase at the bottom, a smectic A one at the opening, and a smectic B phase in-between (for clarity, scattered intensity plots have been shifted in ordinate, according to the place where they were collected in the sample). Peaks related to a lamellar order are denoted (00*l*) and T. Peaks related to the hexagonal parameters a_{hex} and a_{SmB} are denoted (*hk*0). The corresponding rod organizations are also sketched. (b, d) Data for the same sample, obtained on our in-house setup ~5 months latter. (b) Spectrum of the smectic B phase. (c) Corresponding X-ray diffuse scattering along the 6-fold axis of the smectic B organization. (d) High-resolution SAXS enlightening the coexistence of lamellar and hexagonal orders. (e) Microfocus SAXS spectrum collected *in situ* on a wall produced by drying between a substrate and a PDMS mold. The beam size and its position are indicated by the red circle drawn in the inset.

arranged on a hexagon, Fourier transform (FT) of views captured along the GNR main axis confirms the hexagonal intralamella order (see the inset in Figure 3b); a hexagonal lattice parameter, $a_{SmB} = 9.5 \pm 0.2$ nm, can even be extracted. This value is incidentally verified by plotting intensity profiles along lamella cross sections and measuring the curves' periodicity: it yields $a_{SmB} \approx 10$ nm (see the inset in Figure 3f). Finally, from the latter images, a rough estimate of the lamellar order lattice parameter is easy to determine: we find $d_{SmB} \approx 24$ nm.

We next study nanorods self-assembling using SAXS to further unravel the structural properties of the obtained crystal. These bulk experiments are performed by letting suspensions of functionalized GNRs dry at room temperature in ~1.5 mm diameter glass capillaries, the initial particle concentration being $\sim 10^{-8}$ M. Our first high-resolution synchrotron SAXS measurements were achieved on the sample typically 12 h after the drying onset. Powder diffraction patterns are obtained, indicating crystalline domains smaller than the $400 \times 50\,\mu m^2$ beam size. Furthermore, the 500 data sets collected along the tube axis display a continuous evolution of the scattered intensity plots (see Figure 4a). More precisely, at the capillary opening a lamellar structure is characterized by two Bragg peaks at 0.018 and 0.035 $Å^{-1}$. No lateral order between GNRs can be evidenced, and thus this signature is attributed to a smectic A arrangement (SmA) with a repetition distance $d_{SmA} = 35 \pm 2$ nm. Conversely, at the closed end of the tube we find a hexagonal lateral packing (Hex), as indicated by four Bragg peaks at 0.0515, 0.0894, 0.1029, and 0.1375 $Å^{-1}$, with a respective distance ratio of $1:\sqrt{3}:2:\sqrt{7}$. These values correspond to a mean interdistance between nanorods $a_{Hex} = 14.0 \pm 0.3$ nm. In addition, the hexagonal phase spectrum presents an additional diffuse scattering at 0.0405 $Å^{-1}$. Although the latter steadily shifts to the second-order Bragg diffraction of the lamellar phase, it cannot be indexed here as such because of the absence of any first-order signature. Nevertheless, since the discussed peak is associated with a 17 ± 0.5 nm spacing, *i.e.*, $\sim d_{SmA}/2$, we propose to assign it to a half-length translation between adjacent GNRs (see the schemes in Figure 4a). Finally, at the intermediate part of the tube, a higher order phase exhibits scatterings typical of both hexagonal and lamellar order, in agreement with a smectic B arrangement.

It is important to remark that the present SAXS investigations, conducted after only a few hours drying, are not perfectly consistent with SEM observations. Consequently, we hypothesized that the sample was still out-of-equilibrium, and accordingly we have

reanalyzed it on our custom-made setup after complete water evaporation. The capillary content is now more homogeneous, and it exhibits signatures typical of both hexagonal and lamellar order (see Figures 4b and S8). Oriented domains larger than the beam size, *i.e.*, $\sim 300 \times 300\ \mu m^2$, can even be evidenced (see Figure 4b). The 6-fold symmetry is confirmed by the observation of six peaks associated with the first-order scattering by a lateral hexagonal packing along the direction normal to the tube wall (see Figure 4c). Yet, in this orientation the Bragg peaks corresponding to the arrangement perpendicular to the nanorods' main axis cannot be emphasized because the monodomain is very well aligned. Incidentally, this observation agrees with the SEM images collected when drying proceeds between a silicon wafer and a PDMS stamp (see Figure 3e and f): nanorods tend to stand upright on interfaces. High-resolution acquisitions on multidomain areas were then achieved, and they demonstrate the coexistence of two first (00*l*) lamellar peaks and of the (100) hexagonal one (see Figure 4d); we can therefore conclude that GNRs are here also organized according to a smectic B order. For the lattice parameters, one computes from the experimental data $a_{SmB} = 11.3 \pm 0.1$ nm and $d_{SmB} = 24 \pm 1$ nm, both matching quite well the values extracted from FT analysis of SEM images. Furthermore, when comparing the new results with the SAXS measurements conducted on the freshly dried suspension (*i.e.*, a_{Hex} and d_{SmA}, respectively), we note a clear decrease of the interdistances. We attribute this observation to the slow dehydratation of the polyethylene glycol ligands present at the nanorod surface. To summarize, MUDOL GNR self-assembling induced by slow water evaporation in a glass capillary first yields a smectic A/hexagonal polymorphism, which progressively transforms to smectic B local order upon complete drying.

In the absence of any kinetic investigation on the faster drying process involving a thinner film of colloidal suspension confined between a smooth and a topographically patterned surface, the preceding scenario is established only for bulk crystallization. However, we are confident that in both cases the system reaches a similar organization at thermodynamic equilibrium. Indeed, SEM data acquired on GNR walls and SAXS ones collected in a capillary provide results in good agreement. This fact is further confirmed by the $a_{SmB} = 10.3 \pm 0.2$ nm value measured by microfocused SAXS on features dried between a nelophan membrane and a PDMS mold (see Figure 4e). Unfortunately, we could not rely on microfocused WAXS to reinforce the SEM observations of nanorod alignment perpendicular to the substrate[12] because the cubic crystalline system of the GNR colloids does not exhibit split Bragg peaks (see Figure S2). Nonetheless, we estimate that our set of measurements is comprehensive enough to allow a unified description of the most stable structure, *i.e.*, the one obtained after complete dehydratation. The structure of the colloidal crystal should be unique whatever the considered formation mechanism, thus enabling a cross use of SEM and SAXS experiments. Finally, as Tween 20 is introduced only in GNR suspensions employed for wall formation, to definitely validate our methodological approach, we check this surfactant innocuousness with respect to self-assembly. As proved by SEM pictures and SAXS spectra collected on samples with and without the neutral detergent, no adverse effects could be evidenced (respectively compare Figures 3e and S11c as well as the two curves of Figure S9).

To investigate the role of electrostatic interactions in nanorod organization, various particle coatings, at different MUDOL/MUDIC ratios, are examined with respect to the final material morphology. We first used the PDMS stamp drying method. Similarly to the case of pure MUDOL, well-ordered assemblies of smectic B domains are observed by SEM for a 80/20 MUDOL/MUDIC composition (see Figure 5a and b). In contrast, disordered aggregates are obtained when the colloids are functionalized with an equimolar mixture of both ligands (see Figure 5c and d). We next tried to more precisely characterize samples by FT analysis of SEM views. Although many areas of the wall surface exhibit nearly hexagonal packing when MUDIC is present at 20% (see the arrangement of the six peaks in Figure 5b inset), it is very difficult to discern any lattice when the proportions of neutral and negative ligands are equal. Consequently, image autocorrelation appeared a more promising method to evaluate the spacing between nanorods. From the radial profiles issued from circular integration of the processed data, we estimate the colloid interdistance to vary from $a_{SmB}(100/0) \approx 8.9$ nm to $a_{SmB}(80/20) \approx 10.2$ nm when MUDIC is added to MUDOL as to represent one-fifth of the mixture (see Figure 5e and Figure S12). As far as an ordered area could be discovered in the 50/50 MUDOL/MUDIC sample (see Figure S12c), we also could compute $a_{SmB}(50/50) \approx 12.1$ nm. In parallel with the preceding experiments, SAXS measurements are done on GNR suspensions that have been dried in capillaries. Our custom-made setup yields data that unambiguously reinforced SEM observations. In the pure MUDOL case, four peaks are observed, which correspond to a respective distance ratio of $1:\sqrt{3}:2:\sqrt{7}$, which can be indexed in a hexagonal lattice (see Figure 5f). Thereafter, the packing quality decreases when the ratio of negatively charged MUDIC increases, as demonstrated by the broadening of the secondary peaks. At the same time, the first-order peak is shifted to smaller q, indicating that the intercolloid spacing becomes larger; it gains more than 1 nm when the MUDIC content reaches 50%. Finally, assemblies of nanorods capped with various MUDOL/MUDIC mixtures were also analyzed by TEM. Despite the fact that sample preparation

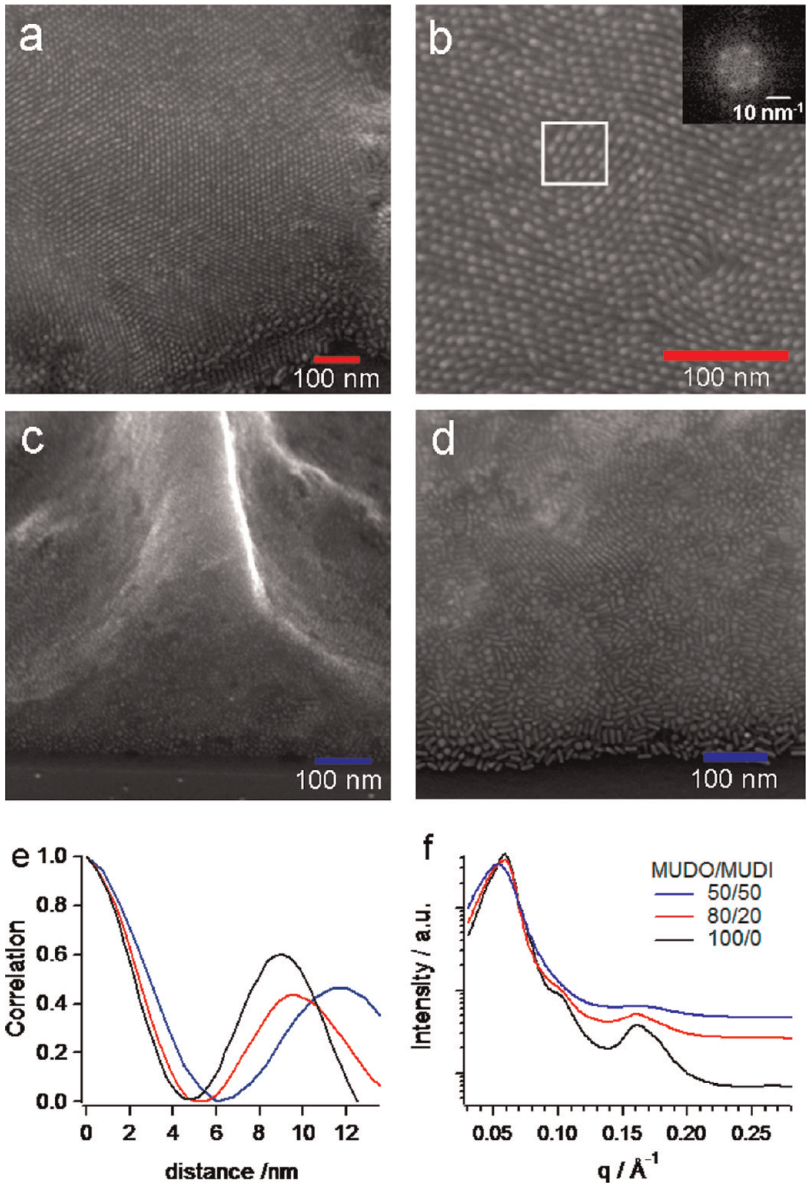

Figure 5. Characterization of self-assemblies resulting from drying suspensions of GNRs capped with different mixtures of neutral and negative alkanethiolates. (a, b) SEM images of the walls produced when evaporation takes place between a silicon substrate and a PDMS stamp and when the MUDOL/MUDIC ratio is equal to 80/20. The inset shows the FT of the area enclosed in the white square. (c, d) SEM images of similar features corresponding to a 50/50 MUDOL/MUDIC ratio. (e) Autocorrelation analysis performed on the SEM views of the structure surface (see Figure S10). Data for three MUDIC percentages are presented: black 0%, red 20%, and blue 50%. (f) SAXS analysis of the solids obtained upon dehydration of colloidal solutions contained in glass capillaries.

here implies a third kind of drying protocol, images evidence already-seen trends: GNRs organize into well-defined side-to-side aggregates, which include several tens of particles for pure MUDOL, 10 of them for 80/20 MUDOL/MUDIC, and only pairs for 50/50 MUDOL/MUDIC (see Figure S4). Therefore, all the experiments prove that mastering nano-objects' surface potential is of foremost importance to obtain organized supracrystals. Additionally, over a given distance range electrostatic repulsion can serve to impose a precisely tuned lattice parameter. However, the strength of this repulsive potential has to be maintained weak enough in order not to inhibit self-assembling. As evidenced by the control observations performed on the "as-synthesized" colloids, which are capped by the sole CTAB, being too strongly charged only results in disordered aggregates (see Figure S11a and b for SEM, Figure S10 for SAXS, and Figure S4a for TEM).

CONCLUSION

We introduced a method opening access to the formation of 3D gold nanorod superstructures having a local smectic B order. We also discussed the importance of surface functionalization, which enables tuning repulsive and attractive forces acting on the GNRs so as to help their self-organization; more precisely,

particles are coated with the neutral MUDOL ligand, optionally supplemented with the negative MUDIC one (up to a few tens of percents). Colloid anisotropy results in a smectic B condensed phase with a lamellar parameter around 25 nm and a hexagonal one around 10 nm, depending on the amount of negatively charged capping agent. We obtain well-defined wall features when the nanorod solution is dried between a smooth surface and a topographically patterned PDMS stamp in the presence of the Tween 20 surfactant. This textured surface allows us to fix a slow and regulated evaporation rate and to define at the millimeter scale the shape of the final nanomaterial. Indeed, our experiments show that the motion of the contact line during drying is strongly affected by the micrometer-size features of the mold. Pinning of the meniscus yields the formation of capillary bridges, which evolve over time to become an engineered superstructure made of 3D walls of smectic B GNRs. Spatially controlled deposition of gold nanoparticles has previously been conducted using either passive processes, based on electrostatic and capillary forces, or active transfer involving PDMS stamps inked with thiolates. However, both strategies lead only to 2D-restricted assemblies.[54]

Microwires were also generated by evaporation of a suspension of 20 nm diameter gold colloids in the interstices of a 2D crystal built of polystyrene latexes.[55] Although the latter method provides an alternative way for shaping self-assemblies of nanoparticles, it appears to be limited in terms of geometries. In comparison, our approach offers a low-cost way to truly order GNRs precisely and reproducibly within 3D macroscopic configurations (in the present case periodic arrays extending over several square millimeters). Our findings could then facilitate the elaboration of functional materials. For example, interesting developments could emerge in SERS or plasmonic detection where crystalline ordering would favor a much higher sensitivity than the one expected from sensors fabricated by classical drying techniques on a smooth substrate.[3,16] Additionally, the manufacturing protocol presented here could be extended to any kind of water-soluble anisotropic colloids provided the optimization of an appropriate chemical coating. For instance, application to semiconductor nanocrystals would be a plus, as they are attractive candidates for both photocatalytic and photovoltaic devices.[56]

METHODS SECTION

Synthesis of Gold Nanorods. Synthesis was achieved relying on a previously described one-pot procedure.[31,33] Particles with an absorption maximum at 750 nm were obtained 20 min after the reducing agent addition. Next, starting with 10 mL of crude reactive mixture, the excess CTAB was removed by two washing cycles, which included centrifugation at 14000*g* for 10 min and pellet dissolution in 10 mL of CTAB prepared at 0.5 mM in Milli-Q water of resistivity 18.2 MΩ. The nanorod concentration was finally derived from the optical density measured at 750 nm and the extinction coefficient provided in the literature.[57] The titer of this stock solution of "as-synthesized" GNRs was found to be $\sim 4 \times 10^{-10}$ M.

GNR Grafting. This was accomplished by simply adding 10 μL of a 10 mM aqueous solution of ligand to 1 mL of the previous colloidal suspension. The mixture was vortexed briefly and then stirred at room temperature for 24 h. The exchange was subsequently controlled by electrophoresis, a 0.5% agarose gel was used, and migration was performed for 45 min in 20 mM borate buffer, pH 8.5, under a 3.3 V·cm^{-1} electric field. After functionalization, all GNR suspensions were employed for self-assembling experiments without any further purification. In order to remove the excess ligand, only FTIR samples were prepared by three dialyses of a 10^{-9} M GNR suspension (1 mL) against an aqueous solution (1 L) containing TMD 8 mixed bed resin (10 g; Sigma).

Transmission Electron Microscopy. TEM was conducted on the JEOL 1400 apparatus of the microscopy platform at Rennes 1 University. Samples were prepared by depositing drops of colloidal suspension at 10^{-9} M onto grids (Formvar/carbon on 300 mesh copper, Agar Scientific) and letting them dry at room temperature for 12 h. The mean length and diameter of the GNRs were determined from the corresponding size histograms, established with the open access ImageJ software.

Small-Angle X-ray Scattering. SAXS measurements were performed on either a custom-made setup[58] or the high brilliance SWING beamline (12 keV) located at the Soleil synchrotron facility.[59] Except in Figure 5c, all samples exhibited powder diffraction patterns; thus, circular integration allowed one to plot the scattering intensity as a function of the radial wave vector $q = 4\pi \sin(\theta)/\lambda$. Self-assembled condensed phases were prepared in 1.3−1.6 mm diameter glass capillaries (Glas-Technik & Konstruktion Müller & Müller OHG). Typically, the GNR suspension was at an initial concentration of $\sim 10^{-8}$ M. It was prepared in 0.5 mM CTAB, and Tween 20 was added only in the control experiment reported in Figure S9; its titer was then 0.1 mM. The still "wet" sample investigated at Soleil was dried for 12 h, and the completely dehydrated samples characterized in Rennes were desiccated for more than 48 h in a box containing phosphore pentoxide (Aldrich).

3D GNR Self-Assembling onto a Solid Substrate. This was carried out by controlled drying of colloidal suspensions between a smooth surface and a topographically patterned one. More precisely, a microtextured stamp was first manufactured in PDMS (Sylgard 184, Dow Corning) relying on standard soft lithography protocols[60] and on a 35 μm deep master mold fabricated in negative photoresist (SU8-2025, Microchem). Two square arrays of 100 μm diameter pillars were used, the lattice parameter being either 175 or 350 μm. Meanwhile, "as-synthesized" or chemically modified GNRs were prepared at 10^{-6} M in 0.5 mM CTAB supplemented with 0.1 mM Tween 20; the latter neutral detergent was always present except in some of the experiments displayed in Figures S6 and S11a and c. A 1 μL droplet of this solution was next casted between the substrate and the elastomeric template. Drying took place at room temperature for about 10 h before the removal of the PDMS cover.

Scanning Electron Microscopy. Images were recorded on a Magellan 400 L (FEI) with settings as follows: acceleration voltage 5 kV, probe current 0.2 nA, working distance 3.9 mm. Features were here obtained by drying the colloidal solutions on ⟨100⟩ silicon wafers of resistivity 1−10 Ω·cm^{-1}. Moreover, to gain insight into the internal structure of GNR self-assemblies, we depended on two tricks. Either we simply cleaved the

samples to allow cross sectional observation, or we broke the walls apart with MM3A-M micromanipulators (Kleindiek Nanotechnik) mounted on a Leo 1430 microscope (Zeiss). Fourier transform computation was achieved with ImageJ, whereas autocorrelation analysis was undertaken relying on DigitalMicrograph (Gatan).

Conflict of Interest: The authors declare no competing financial interest.

Acknowledgment. V.M.A. and C.G. thank the Agence Nationale de la Recherche (ANR) for financial support through the "BioModulator" grant obtained on the 2008 PNANO program. V.M.A. and F.A. acknowledge the Direction Générale de l'Armement (DGA), the Centre National de la Recherche Scientifique (CNRS), and the Région Bretagne for the Ph.D. fellowships of C. H., M.P., and T.B. We are also indebted to A. Burel (TEM Mric-UMS 3480-Biosit-Université de Rennes1 platform) for her technical expertise in TEM, to G. Hwang and L. Couraud (LPN-CNRS) for conducting the micromanipulators, and to C. Meriadec (IPR-CNRS) and F. Meneau (Swing, SOLEIL) for high-quality assistance with X-ray experiments. We are grateful for the access to the SOLEIL synchrotron radiation facilities, where preliminary experiments were performed.

Supporting Information Available: This section includes TEM size histogram of GNRs (Figure S1), WAXS spectrum of a GNRs suspension dried in a glass capillary (Figure S2), absorbance spectra of GNRs during the exchange of CTAB for MUDOL (Figure S3), TEM images of GNRs capped with CTAB or different MUDIC/MUDOL ratios (Figure S4), SEM images of a MUDOL GNR suspension dried on a wafer without using any PDMS mold (Figure S5), optical micrographs of the GNR features obtained while drying colloidal suspensions between a mold and a substrate with and without Tween 20 and for both CTAB and MUDOL coating (Figure S6), SEM image of the micromanipulator (Figure S7), SAXS spectra collected for the MUDOL GNR sample after complete drying in a glass capillary (Figure S8), SAXS spectra of MUDOL GNRs after drying in glass capillaries in the presence or absence of Tween 20 (Figure S9), SAXS spectra of CTAB GNRs and MUDOL GNRs after drying in glass capillaries (Figure S10), SEM images of GNR features obtained while drying colloidal suspensions between a mold and a substrate with and without Tween 20 and for both CTAB and MUDOL coating (Figure S11), SEM images of the wall surface for GNRs capped with different ratios of MUDIC/MUDOL ligands (Figure S12), SEM images of features obtained while drying a MUDOL GNR suspension between a substrate and a mold where pillars are not spaced by 175 but 350 μm (Figure S13). This material is available free of charge *via* the Internet at http://pubs.acs.org.

REFERENCES AND NOTES

1. Link, S.; El-Sayed, M. A. Optical Properties and Ultrafast Dynamics of Metallic Nanocrystals. *Annu. Rev. Phys. Chem.* **2003**, *54*, 331–366.
2. Jones, M. R.; Osberg, K. D.; Macfarlane, R. J.; Langille, M. R.; Mirkin, C. A. Templated Techniques for the Synthesis and Assembly of Plasmonic Nanostructures. *Chem. Soc. Rev.* **2011**, *111*, 3736–3827.
3. Stewart, M. E.; Anderton, C. R.; Thompson, L. B.; Maria, J.; Gray, S. K.; Rogers, J. A.; Nuzzo, R. G. Nanostructured Plasmonic Sensors. *Chem. Soc. Rev.* **2008**, *108*, 494–521.
4. Noginov, M. A.; Zhu, G.; Belgrave, A. M.; Bakker, R.; Shalaev, V. M.; Narimanov, E. E.; Stout, S.; Herz, E.; Suteewong, T.; Wiesner, U. Demonstration of a Spaser-Based Nanolaser. *Nature* **2009**, *460*, 1110–1112.
5. Cattoni, A.; Ghenuche, P.; Haghiri-Gosnet, A.-M.; Decanini, D.; Chen, J.; Pelouard, J.-L.; Collin, S. Plasmonic Nanocavities for Biosensing Fabricated by Soft UV Nanoimprint Lithography. *Nano Lett.* **2011**, *11*, 3557–3563.
6. Onsager, L. The Effects of Shape on the Interaction Between Colloidal Particles. *Ann. N.Y. Acad. Sci.* **1949**, *51*, 627–659.
7. Liu, K.; Zhao, N.; Kumacheva, E. Self-Assembly of Inorganic Nanorods. *Chem. Soc. Rev.* **2011**, *40*, 656–671.
8. Nikoobakht, B.; Wang, Z. L.; El-Sayed, M. A. Self-Assembly of Gold Nanorods. *J. Phys. Chem. B* **2000**, *104*, 8635–8640.
9. Murphy, C. J.; Sau, T. K.; Gole, A. M.; Orendorff, C. J.; Gao, J.; Gou, L.; Hunyadi, S. E.; Li, T. Anisotropic Metal Nanoparticles: Synthesis, Assembly, and Optical Applications. *J. Phys. Chem. B* **2005**, *109*, 13857–13870.
10. Jana, N. R. Shape Effect in Nanoparticle Self-Assembly. *Angew. Chem., Int. Ed.* **2004**, *43*, 1536–1540.
11. Link, S.; El-Sayed, M. A. Spectral Properties and Relaxation Dynamics of Surface Plasmon Electronic Oscillations in Gold and Silver Nanodots and Nanorods. *J. Phys. Chem. B* **1999**, *103*, 8410–8426.
12. Zanella, M.; Gomes, R.; Povia, M.; Giannini, C.; Zhang, Y.; Riskin, A.; Van Bael, M.; Hens, Z.; Manna, L. Self-Assembled Multilayers of Vertically Aligned Semiconductor Nanorods on Device-Scale Areas. *Adv. Mater.* **2011**, *23*, 2205–2209.
13. Eustis, S.; El-Sayed, M. Aspect Ratio Dependence of the Enhanced Fluorescence Intensity of Gold Nanorods: Experimental and Simulation Study. *J. Phys. Chem. B* **2005**, *109*, 16350–16356.
14. Tripathy, S.; Marty, R.; Lin, V. K.; Teo, S. L.; Ye, E.; Arbouet, A.; Saviot, L.; Girard, C.; Han, M. Y.; Mlayah, A. Acousto-Plasmonic and Surface-Enhanced Raman Scattering Properties of Coupled Gold Nanospheres/Nanodisk Trimers. *Nano Lett.* **2011**, *11*, 431–437.
15. Kumar, J.; Thomas, K. G. Surface-Enhanced Raman Spectroscopy: Investigations at the Nanorod Edges and Dimer Junctions. *J. Phys. Chem. Lett.* **2011**, 610–615.
16. Alvarez-Puebla, R. A.; Agarwal, A.; Manna, P.; Khanal, B. P.; Aldeanueva-Potel, P.; Carbó-Argibay, E.; Pazos-Pérez, N.; Vigderman, L.; Zubarev, E. R.; Kotov, N. A.; *et al*. Gold Nanorods 3D-Supercrystals as Surface Enhanced Raman Scattering Spectroscopy Substrates for the Rapid Detection of Scrambled Prions. *Proc. Natl. Acad. Sci.* **2011**, *108*, 8157–8161.
17. Baranov, D.; Manna, L.; Kanaras, A. G. Chemically-Induced Self Assembly of Spherical and Anisoptropic Nanocrystals. *J. Mater. Chem.* **2011**, *21*, 16694–16703.
18. Cortie, M. B.; McDonagh, A. M. Synthesis and Optical Properties of Hybrid and Alloy Plasmonic Nanoparticles. *Chem. Soc. Rev.* **2011**, *111*, 3713–3735.
19. Huang, X.; Neretina, S.; El-Sayed, M. A. Gold Nanorods: From Synthesis and Properties to Biological and Biomedical Applications. *Adv. Mater.* **2009**, *21*, 4880–4910.
20. Sau, T. K.; Rogach, A. L.; Jäckel, F.; Klar, T. A.; Feldmann, J. Properties and Applications of Colloidal Nonspherical Noble Metal Nanoparticles. *Adv. Mater.* **2010**, *22*, 1805–1825.
21. Romo-Herrera, J. M.; Alvarez-Puebla, R. A.; Liz-Marzan, L. M. Controlled Assembly of Plasmonic Colloidal Nanoparticle Clusters. *Nanoscale* **2011**, *3*, 1304–1315.
22. Shevchenko, E. V.; Talapin, D. V.; Kotov, N. A.; O'Brien, S.; Murray, C. B. Structural Diversity in Binary Nanoparticle Superlattices. *Nature* **2006**, *439*, 55–59.
23. Nie, Z. H.; Fava, D.; Rubinstein, M.; Kumacheva, E. Supramolecular Assembly of Gold Nanorods End-Terminated with Polymer "Pom-Poms": Effect of Pom-Pom Structure on the Association Modes. *J. Am. Chem. Soc.* **2008**, *130*, 3683–3689.
24. Dong, A.; Chen, J.; Vora, P. M.; Kikkawa, J. M.; Murray, C. B. Binary Nanocrystal Superlattice Membranes Self-Assembled at the Liquid-Air Interface. *Nature* **2010**, *466*, 474–477.
25. Jana, N. R. Shape Effect in Nanoparticle Self-Assembly. *Angew. Chem., Int. Ed.* **2004**, *43*, 1536–1540.
26. Nie, Z. H.; Petukhova, A.; Kumacheva, E. Properties and Emerging Applications of Self-Assembled Structures Made from Inorganic Nanoparticles. *Nat. Nanotechnol.* **2010**, *5*, 15–25.
27. Titov, A. V.; Kral, P. *Nano Lett.* **2008**, *8*, 3605–3612.
28. Zanella, M.; Bertoni, G.; Franchini, I. R.; Brescia, R.; Baranov, D.; Manna, L. Assembly of Shape-Controlled Nanocrystals by Depletion Attraction. *Chem. Commun.* **2011**, *47*, 203–205.
29. Baranov, D.; Fiore, A.; van Huis, M.; Giannini, C.; Falqui, A.; Lafont, U.; Zandbergen, H.; Zanella, M.; Cingolani, R.; Manna,

L. Assembly of Colloidal Semiconductor Nanorods in Solution by Depletion Attraction. *Nano Lett.* **2010**, *10*, 743–749.
30. Walker, D. A.; Browne, K. P.; Kowalczyk, B.; Grzybowski, B. A. Self-Assembly of Nanotriangle Superlattices Facilitated by Repulsive Electrostatic Interactions. *Angew. Chem., Int. Ed.* **2010**, *49*, 6760–6763.
31. Jana, N. R.; Gearheart, L.; Murphy, C. J. Seed-Mediated Growth Approach for Shape-Controlled Synthesis of Spheroidal and Rod-like Gold Nanoparticles Using a Surfactant Template. *Adv. Mater.* **2001**, *13*, 1389–1393.
32. Hubert, F.; Testard, F.; Spalla, O. Cetyltrimethylammonium Bromide Silver Complex as the Capping Agent of Gold Nanorods. *Langmuir* **2008**, *24*, 9219–9222.
33. Jana, N. R. Gram-Scale Synthesis of Soluble, Near-Monodisperse Gold Nanorods and Other Anisotropic Nanoparticles. *Small* **2005**, *1*, 875–882.
34. Murphy, C. J.; Thompson, L. B.; Chernak, D. J.; Yang, J. A.; Sivapalan, S. T.; Boulos, S. P.; Huang, J.; Alkilany, A. M.; Sisco, P. N. Gold Nanorod Crystal Growth: From Seed-Mediated Synthesis to Nanoscale Sculpting. *Curr. Opin. Colloid Interface Sci.* **2011**, *16*, 128–134.
35. Sreeprasad, T. S.; Samal, A. K.; Pradeep, T. One-, Two-, and Three-Dimensional Superstructures of Gold Nanorods Induced by Dimercaptosuccinic Acid. *Langmuir* **2008**, *24*, 4589–4599.
36. Park, S.; Sinha, N.; Hamad-Schifferli, K. Effective Size and Zeta Potential of Nanorods by Ferguson Analysis. *Langmuir* **2010**, *26*, 13071–13075.
37. Murphy, C. J.; Thompson, L. B.; Alkilany, A. M.; Sisco, P. N.; Boulos, S. P.; Sivapalan, S. T.; Yang, J. A.; Chernak, D. J.; Huang, J. The Many Faces of Gold Nanorods. *J. Phys. Chem. Lett.* **2010**, 2867–2875.
38. Jones, M. R.; Macfarlane, R. J.; Lee, B.; Zhang, J.; Young, K. L.; Senesi, A. J.; Mirkin, C. A. DNA-Nanoparticle Superlattices Formed from Anisotropic Building Blocks. *Nat. Mater.* **2010**, *9*, 913–917.
39. Dujardin, E.; Hsin, L.-B.; Wang, C. R. C.; Mann, S. DNA-Driven Self-Assembly of Gold Nanorods. *Chem. Commun.* **2001**, 1264–1265.
40. Caswell, K. K.; Wilson, J. N.; Bunz, U. H. F.; Murphy, C. J. Preferential End-to-End Assembly of Gold Nanorods by Biotin-Streptavidin Connectors. *J. Am. Chem. Soc.* **2003**, *125*, 13914–13915.
41. Nie, Z.; Fava, D.; Kumacheva, E.; Zou, S.; Walker, G. C.; Rubinstein, M. Self-Assembly of Metal-Polymer Analogues of Amphiphilic Triblock Copolymers. *Nat. Mater.* **2007**, *6*, 609–614.
42. Murphy, C. J. *Nanoparticles Asssemblies and Superstructures*; CRC Press, 2005.
43. Ming, T.; Kou, X.; Chen, H.; Wang, T.; Tam, H.-L.; Cheah, K.-W.; Chen, J.-Y.; Wang, J. Ordered Gold Nanostructure Assemblies Formed by Droplet Evaporation. *Angew. Chem., Int. Ed.* **2008**, *120*, 9831–9836.
44. Valiokas, R. n.; Svedhem, S.; Svensson, S. C. T.; Liedberg, B. Self-Assembled Monolayers of Oligo(ethylene glycol)-Terminated and Amide Group Containing Alkanethiolates on Gold. *Langmuir* **1999**, *15*, 3390–3394.
45. Xie, Y.; Guo, S.; Ji, Y.; Guo, C.; Liu, X.; Chen, Z.; Wu, X.; Liu, Q. Self-Assembly of Gold Nanorods into Symmetric Superlattices Directed by OH-Terminated Hexa(ethylene glycol) Alkanethiol. *Langmuir* **2011**, *27*, 11394–11400.
46. Svedhem, S.; Hollander, C.-Å.; Shi, J.; Konradsson, P.; Liedberg, B.; Svensson, S. C. T. Synthesis of a Series of Oligo(ethylene glycol)-Terminated Alkanethiol Amides Designed to Address Structure and Stability of Biosensing Interfaces. *J. Org. Chem.* **2001**, *66*, 4494–4503.
47. Nuzzo, R. G.; Fusco, F. A.; Allara, D. L. Spontaneously Organized Molecular Assemblies. 3. Preparation and Properties of Solution Adsorbed Monolayers of Organic Disulfides on Gold Surfaces. *J. Am. Chem. Soc.* **1987**, *109*, 2358–2368.
48. Pierrat, S.; Zins, I.; Breivogel, A.; Sonnichsen, C. Self-Assembly of Small Gold Colloids with Functionalized Gold Nanorods. *Nano Lett.* **2007**, *7*, 259–263.
49. Dinca, V.; Kasotakis, E.; Catherine, J.; Mourka, A.; Ranella, A.; Ovsianikov, A.; Chichkov, B. N.; Farsari, M.; Mitraki, A.; Fotakis, C. Directed Three-Dimensional Patterning of Self-Assembled Peptide Fibrils. *Nano Lett.* **2007**, *8*, 538–543.
50. Kang, S. H.; Grinthal, A.; Aizenberg, J. Meniscus Litography: Evaporation-Induced Self Organization of Pillar Arrays into Moiré Patterns. *Phys. Rev. Lett.* **2011**, *107*, 177802.
51. Pokroy, B.; Kang, S. H.; Mahadevan, L.; Aizenberg, J. Self-Organization of a Mesoscale Bristle into Ordered Hierarchical Helical Assemblies. *Science* **2009**, *323*, 237–240.
52. Courbin, L.; Denieul, E.; Dressaire, E.; Roper, M.; Adjari, A.; Stone, H. A. Imbibition by Polygonal Spreading on Microdecorated Surfaces. *Nat. Mater.* **2007**, *6*, 661–664.
53. Deegan, R. D.; Bakajin, O.; Dupont, T. F.; Huber, G.; Nagel, S. R.; Witten, T. A. Capillary Flow as the Cause of Ring Stains from Dried Liquid Drops. *Nature* **1997**, *389*, 827–829.
54. Aizenberg, J.; Braun, P. V.; Wiltzius, P. Colloid Deposition Controlled by Electrostatic and Capillary Forces. *Phys. Rev. Lett.* **2000**, *84*, 2997–3000.
55. Vakarelski, I. U.; Chan, D. Y. C.; Nonoguchi, T.; Shinto, H.; Higashitani, K. Assembly of Gold Nanoparticles into Microwire Networks Induced by Drying Liquid Bridges. *Phys. Rev. Lett.* **2009**, *102*, 058303.
56. Shemesh, Y.; Macdonald, J. E.; Menagen, G.; Banin, U. Synthesis and Photocatalytic Properties of a Family of CdS-PdX Hybrid Nanoparticles. *Angew. Chem., Int. Ed.* **2011**, *50*, 1185–1189.
57. Liao, H.; Hafner, J. H. Gold Nanorod Bioconjugates. *Chem. Mater.* **2005**, *17*, 4636–4641.
58. van Grondelle, W.; López Iglesias, C.; Coll, E.; Artzner, F.; Paternostre, M.; Lacombe, F.; Cardus, M.; Martinez, G.; Montes, M.; Cherif-Cheikh, R.; *et al*. Spontaneous Fibrillation of the Native Neuropeptide Hormone Somatostatin-14. *J. Struct. Biol.* **2007**, *160*, 211–223.
59. Henry, E.; Dif, A.; Schmutz, M.; Legoff, L.; Amblard, F.; Marchi-Artzner, V.; Artzner, F. Crystallization of Fluorescent Quantum Dots within a Three-Dimensional Bio-Organic Template of Actin Filaments and Lipid Membranes. *Nano Lett.* **2011**, *11*, 5443–5448.
60. McDonald, J. C.; Duffy, D. C.; Anderson, J. R. Fabrication of Microfluidic Systems in Poly(dimethylsiloxane). *Electrophoresis* **2000**, *21*, 27–40.